Journal of Magnetic Resonance 273 (2016) 65–72

Contents lists available at ScienceDirect

Journal of Magnetic Resonance

journal homepage: www.elsevier.com/locate/jmr

# Multi-turn multi-gap transmission line resonators – Concept, design and first implementation at 4.7 T and 7 T

Roberta Frass-Kriegl [a,b,*], Elmar Laistler [a,b], Sajad Hosseinnezhadian [a,b,c], Albrecht Ingo Schmid [a,b], Ewald Moser [a,b], Marie Poirier-Quinot [c], Luc Darrasse [c], Jean-Christophe Ginefri [c]

[a] Center for Medical Physics and Biomedical Engineering, Medical University of Vienna, Währinger Gürtel 18-20, 1090 Vienna, Austria
[b] MR Centre of Excellence, Medical University of Vienna, Lazarettgasse 14, 1090 Vienna, Austria
[c] Laboratoire d'Imagerie par Résonance Magnétique Médicale et Multi-Modalités (IR4M), Université Paris-Sud, CNRS, Université Paris-Saclay, Bâtiment 220, Rue André Ampère, 91405 Orsay, France

ARTICLE INFO

*Article history:*
Received 25 May 2016
Revised 18 August 2016
Accepted 9 October 2016
Available online 11 October 2016

*Keywords:*
RF coil
Surface coil
Transmission line resonator
EM simulation
$B_1$ mapping
High-field MRI

ABSTRACT

A novel design scheme for monolithic transmission line resonators (TLRs) is presented - the multi-turn multi-gap TLR (MTMG-TLR) design. The MTMG-TLR design enables the construction of TLRs with multiple turns and multiple gaps. This presents an additional degree of freedom in tuning self-resonant TLRs, as their resonance frequency is fully determined by the coil geometry (e.g. diameter, number of turns, conductor width, etc.). The novel design is evaluated at 4.7 T and 7 T by simulations and experiments, where it is demonstrated that MTMG-TLRs can be used for MRI, and that the $B_1$ distribution of MTMG-TLRs strongly depends on the number and distribution of turns. A comparison to conventional loop coils revealed that the $B_1$ performance of MTMG-TLRs is comparable to a loop coil with the same mean diameter; however, lower 10g SAR values were found for MTMG-TLRs. The MTMG-TLR design is expected to bring most benefits at high static field, where it allows for independent size and frequency selection, which cannot be achieved with standard TLR design. However, it also enables more accurate geometric optimization at low static field. Thereby, the MTMG-TLR design preserves the intrinsic advantages of TLRs, i.e. mechanical flexibility, high SAR efficiency, mass production, and coil miniaturization.


## 1. Introduction

Since their introduction to MRI, monolithic transmission line resonators (TLRs) [1–3] have been applied as highly sensitive surface probes in several dedicated studies concerning wireless implanted coils [4], cryogenic coils [5] and miniature superconducting coils [6].

TLRs consist of two circular conducting bands intersected by diagonally opposite gaps and deposited on both sides of a low-loss dielectric substrate. They are self-resonant and can be tuned over a wide range of MR frequencies without the use of lumped elements by adjusting the geometrical parameters of the TLR, such as substrate thickness and permittivity, conductor width, number of turns, and number of gaps. The electromagnetic behavior of the TLR can be described using a dual description of the currents flowing in the resonator's winding [2,3]. On the one hand, wave propagation analysis is used to describe the differential mode current, resulting from two anti-symmetrical currents equal in magnitude but with opposite signs. The differential mode current is responsible for the self-resonance of the transmission line. On the other hand, Kirchhoff's law is used to analyze the common mode current, resulting from two symmetrical currents equal in sign and magnitude. The common mode current creates an RF magnetic field outside the substrate and is responsible for the magnetic coupling with the environment. The combined analysis of current modes in the transmission line provides the resonance condition of the TLR.

$$\frac{L_{\mathrm{tot}}\omega_0}{4n_{\mathrm{g}}Z_0}\tan\left(\frac{\omega_0\sqrt{\varepsilon}l}{4n_{\mathrm{g}}c}\right)=1 \tag{1}$$

The resonance condition contains the angular resonance frequency $\omega_0$, the total TLR inductance $L_{\mathrm{tot}}$, the number of gaps $n_{\mathrm{g}}$, the characteristic transmission line impedance $Z_0$, the relative permittivity of the substrate $\varepsilon$, the total length of the conductor on one side of the substrate $l$ (including gaps), and the vacuum speed of light $c$. $L_{\mathrm{tot}}$, which is the sum of the individual inductances of the

* Corresponding author at: Center for Medical Physics and Biomedical Engineering, Medical University of Vienna, Währinger Gürtel 18-20, 1090 Vienna, Austria.
*E-mail address:* roberta.frass@meduniwien.ac.at (R. Frass-Kriegl).

http://dx.doi.org/10.1016/j.jmr.2016.10.008
1090-7807/

windings on both sides of the substrate and their respective mutual inductance, as well as $Z_0$ can be calculated by semiempirical models; respective equations are given in [3].

TLRs can be fabricated on thin and flexible substrates in order to enable form-fitting of the coils to different sample geometries, providing substantial gain in signal-to-noise ratio (SNR) as compared to planar coils [4]. Also, the accurate and highly reproducible fabrication process by photo-lithographic etching, and the absence of lumped elements, such as tuning capacitors, make the TLR design especially favorable for miniaturized RF coils [4,5]. The precision required for the fabrication process depends on the feature size of the designed structures, where the exact alignment of the conductors on top and bottom side of the substrate is most critical. Tolerances presented by standard photolithography systems are in general sufficient. In comparison to widely used miniaturized spiral surface coils [7], TLRs provide better confinement of electrical fields within the dielectric substrate. Compared to conventional microstrip coils [8], TLRs do not rely on lumped element capacitors for miniaturization at low field strength, but can be built in a purely monolithic fashion. Further, if an inductive matching strategy is pursued, no solder joints have to be made directly on the coil, promoting the use of TLRs as superconducting surface coils that exhibit very low internal coil noise and thus achieve a high SNR, which allows for high resolution imaging even at intermediate field strength [6]. While single-sided monolithic coil designs, like for instance the racetrack design [9], are often limited to ultra-high field strength, because the achievable interdigital capacitance is small, TLRs can also be tuned to low frequencies due to their double-sided design.

According to these properties, TLRs have mostly been applied in the fields of miniaturized and superconducting RF coils, however, lacking extension to other domains like biomedical MR applications on humans. Most of these applications require a large field-of-view (FOV) in the order of tens of cm covering the organ to be investigated and, therefore, call for large sized coils or coil arrays [10]. Despite the additional advantages provided by array technology, simple transmit-receive surface coils are still widely used for their simplicity in design and fabrication, and their compatibility with MR scanners featuring only a single RF channel. Surface loop coils play an important role at low and intermediate field strength, but they are of particular interest for ultra-high field MRI applications due to the lack of efficient whole body coils.

Although, (ultra-) high field studies requiring a large FOV represent a promising area of application for TLRs, they are not regularly applied in this domain because of design limitations. Up to now, TLRs exist in two different configurations: (1) with a single turn and one or several gaps per conductor (Fig. 1a and b), and (2) with multiple turns but only a single gap per conductor (Fig. 1c). Applications calling for large high frequency resonators could not be addressed by multi-turn TLR design, so far, because of the intrinsically low resonance frequencies of large multi-turn TLRs. High frequency resonators require a small equivalent inductance and/or capacitance, consequently setting a maximum diameter or a maximum number of turns for the TLR. Contrarily, for a given size, the resulting equivalent inductance and capacitance of the TLR limit the highest achievable frequency. Only for single-turn multi-gap TLRs, the equivalent capacitance can be reduced by increasing the number of gaps to increase the resonance frequency; however, this way, only a discrete spectrum of resonance frequencies can be accessed due to practical limitations for other design parameters, e.g. the substrate properties. Besides these limitations for large, high-frequency TLRs, also traditional TLR applications suffer from design constrictions; the number of available substrate materials and thicknesses is limited, which can pose a limit on other parameters like TLR diameter, number of turns, and conductor width.

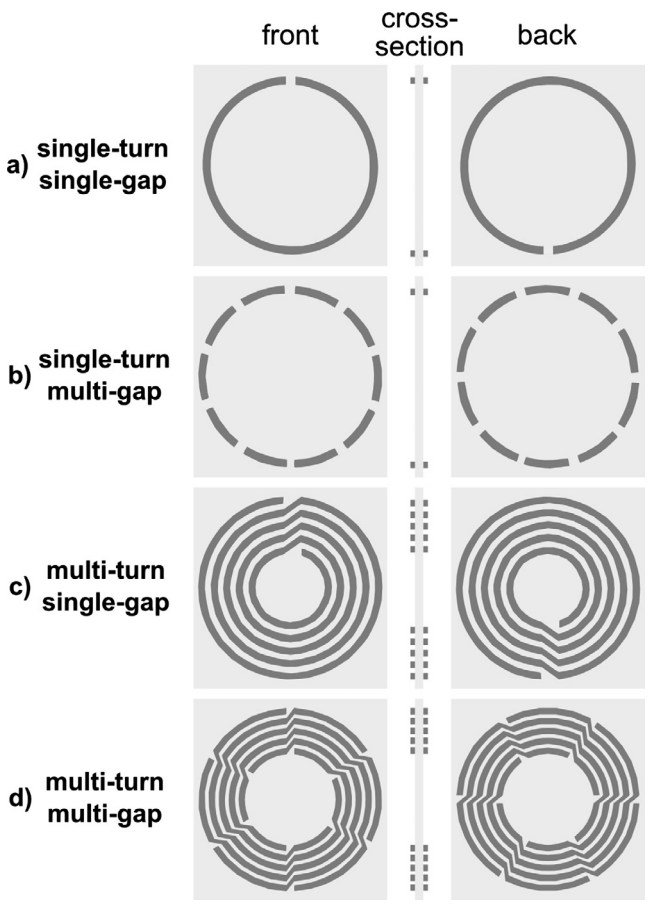


**Fig. 1.** Different TLR designs. (a) Single-turn single-gap TLR, (b) single-turn multi-gap TLR, (c) multi-turn single-gap TLR, (d) multi-turn multi-gap TLR.

In this work, a novel concept based on the existing TLR design is proposed that enables the realization of TLRs with multiple turns and multiple gaps at the same time. The novel multi-turn multi-gap TLR (MTMG-TLR) design brings an additional degree of freedom and helps to overcome current limitations in efficiently designing TLRs for various applications.

## 2. Methods

### 2.1. Multi-turn multi-gap TLR design

An MTMG-TLR (Fig. 1d) is composed of several conductive strips ranging from the outermost to the innermost turn, partially overlapping with conductive strips on the other side of the substrate. The possibility to choose the number of gaps independently from the number of turns provides an additional degree of freedom in TLR design. Despite this innovation, the analytical model yielding a simple expression for the resonance condition of TLRs (Eq. (1)), derived in early publications [2,3], is still valid for MTMG-TLRs, as no restriction regarding the number of turns or gaps is made in the derivation.

The novel MTMG-TLR design was first applied in a prototype study conducted using a 4.7 T small animal MR imaging system. An easily accessible, experimental MR scanner at intermediate field strength was chosen for the first tests to facilitate handling and the detection of potential design flaws. After providing the proof-of-principle at 4.7 T, the applicability of the MTMG-TLR design was investigated at ultra-high field strength, i.e. a regime

that could not be addressed with multi-turn TLRs before. Therefore, a comparison study at 7 T was performed, containing five different MTMG-TLRs and three conventional loop coils.

### 2.2. Prototype study at 4.7 T

#### 2.2.1. Coil design

Using Eq. (1), an MTMG-TLR with 6 turns and 4 gaps ("6t4g") resonating at approximately 200 MHz (i.e. $^1$H @ 4.7 T) was designed. The following geometric parameters were used: external diameter $d_{ext}$ = 42 mm, conductor width $w$ = 1.25 mm, spacing between turns $p$ = 1.3 mm, substrate thickness $h$ = 0.51 mm, substrate material = PTFE, substrate permittivity $\varepsilon$ = 2.05. The layout is shown in Fig. 2a. The MTMG-TLR can be fine-tuned and matched using a pick-up loop with a diameter of 30 mm placed coaxially at a distance of 20 mm employing the resonant inductive matching technique [11]. With this matching technique, the TLR and a tuned pick-up loop are operated in over-coupled mode where the $S_{11}$ curve shows two resonance peaks. If the initial resonance frequency of the MTMG-TLR is higher than the Larmor frequency, the pick-up loop has to be tuned above the MTMG-TLR in order to shift the lower resonance peak of the coupled two-coil system "down" to the Larmor frequency (and vice versa for too low initial resonance frequency of the MTMG-TLR). In addition, adjustable matching capacitors are placed on the pick-up loop in order to perform impedance matching without varying the distance between MTMG-TLR and pick-up loop, which makes the system mechanically more stable. Tuning and matching was performed on the bench by manually adjusting the variable capacitors on the pick-up loop.

#### 2.2.2. Experimental evaluation

The prototype MTMG-TLR was fabricated in-house from double-sided CuFlon® microwave substrate (Polyflon Company, Norwalk, USA) by photolithographic etching. Upon fabrication, the resonance frequency, and quality factor $Q$ were measured using the single-loop probe method [12] in four different configurations: (1) unloaded, flat MTMG-TLR, (2) flat MTMG-TLR loaded by a flat saline phantom (5 g/L NaCl, 60 × 60 × 30 mm$^3$), (3) flat MTMG-TLR loaded by a cylindrical saline phantom (5 g/L NaCl, 45 mm diameter, 175 mm long), (4) MTMG-TLR wrapped around the cylindrical phantom (Fig. 2b).

Further, to investigate the usability of the novel TLR design for MRI, MR imaging was performed in transmit/receive mode on a 4.7 T small animal MR imaging system (BioSpec USR47/40, Bruker BioSpin, Billerica, USA). Transversal 3D gradient-echo images

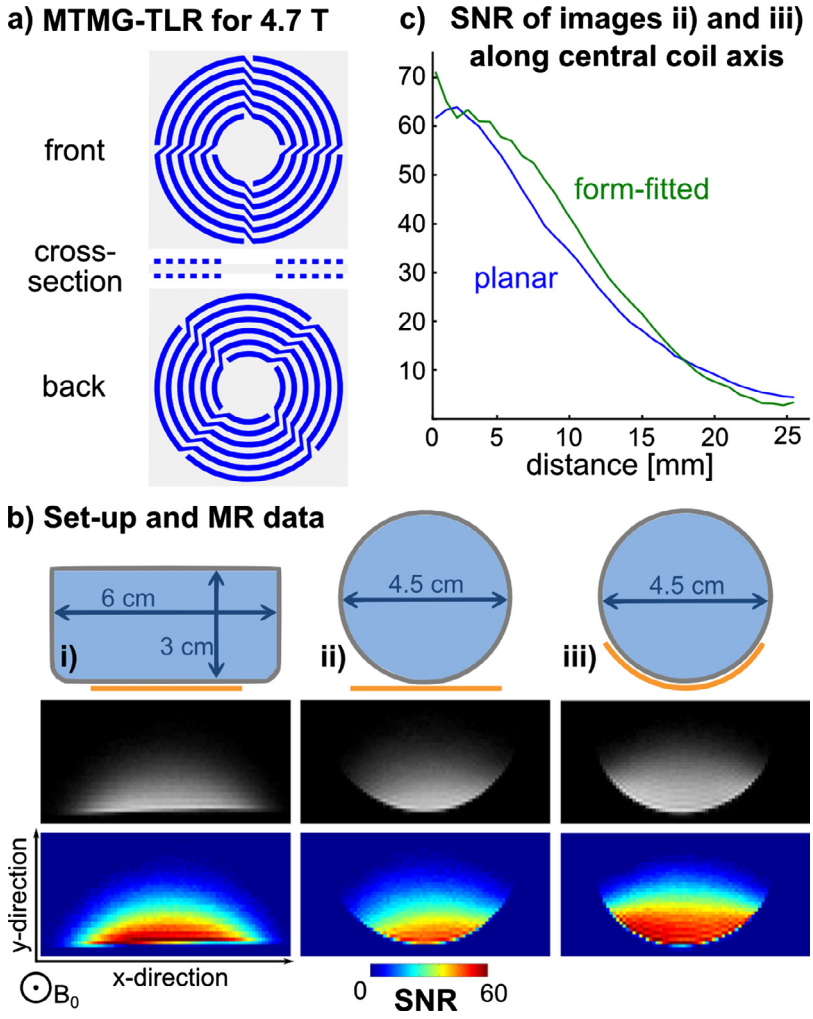


**Fig. 2.** MR imaging results of the MTMG-TLR prototype study at 4.7 T. (a) Coil design. (b) Set-up and MRI data with the position of the coil marked in orange. (i) Flat MTMG-TLR with a phantom with planar surface. (ii) Flat MTMG-TLR with a cylindrical phantom. (iii) MTMG-TLR wrapped around the cylindrical phantom. Images and SNR maps are scaled to the same spatial dimensions as the drawings of the coil set-up. (c) SNR comparison: form-fitted (green, b-iii) versus the non-form-fitted (blue, b-ii) configuration. (For interpretation of the references to color in this figure legend, the reader is referred to the web version of this article.)

($T_R/T_E$ = 100/0.74 ms, $T_{acq}$ = 20 min, 750 × 750 × 500 μm$^3$ nominal resolution, 80 × 80 × 10 mm$^3$ FOV) were acquired in configurations (2)-(4), as described above. The SNR between form-fitted and non-form-fitted configuration was compared.

### 2.3. Comparison study at 7 T

#### 2.3.1. Coil design

After providing the proof-of-principle at 4.7 T, the applicability of the MTMG-TLR design was investigated at ultra-high field strength. Therefore, five different MTMG-TLRs with an external diameter of 10 cm were designed for $^1$H imaging at 7 T, i.e. 300 MHz. The geometric parameters of the five MTMG-TLRs are given in Table 1. They are labeled 4t10g-3cm, 5t14g-4cm, 2t6g-5cm, 5t16g-6cm, and 2t6g-8cm according to their respective number of turns and gaps, as well as their approximate inner diameter.

In addition to the designed MTMG-TLRs, also three conventional surface coils with diameters of 7 cm, 8 cm, and 9 cm were studied for comparison. The coils were formed from 1.5 mm thick copper wire, and intersected by four segmentation capacitors. Standard chip capacitor values (CPX series, Temex Ceramics, Pessac, France) were chosen in a way to resonate the loops in a range of ±3% around the Larmor frequency. The resonant inductive matching technique, as described above, with a 5 cm pick-up loop placed 3 cm above the imaging coil was employed for fine-tuning and matching of all investigated coils, i.e. MTMG-TLRs and loops.

#### 2.3.2. 3D electro-magnetic simulations

The performance of the MTMG-TLRs and the loop coils was evaluated by 3D electro-magnetic simulations (Remcom XFdtd 7.4, State College, PA) in combination with circuit co-simulation (Keysight ADS, Santa Clara, CA) [13,14]. 3D CAD models of the coils together with the pickup-loop and a block phantom (244 × 244 × 150 mm$^3$, electrical conductivity $\sigma$ = 0.59 S/m, relative permittivity $\varepsilon$ = 75) were generated. All coils were modeled as perfect electric conductors; also losses from lumped element capacitors and substrate material were neglected, as sample losses were expected to clearly dominate over coil losses for the investigated coil sizes at 300 MHz [15]. This assumption was confirmed by measurements of the quality factor (see section on experimental evaluation). A rectangular mesh with a minimum cell size of 0.9 × 0.2 × 0.9 mm$^3$ (within the dielectric substrate) and a maximum cell size of 2 × 3 × 2 mm$^3$ was used. Two 50-Ohm ports were placed in the pick-up loop. For the loop coils, four additional ports were used to represent the segmentation capacitors. S-parameters of these multi-port systems, the prototype magnetic field $B_1$ and electric field E produced by the coils, as well as the current density J along the conductors were simulated. In circuit co-simulation, the 50-Ohm ports were replaced by corresponding capacitors for tuning and impedance matching. Co-simulation yielded S-parameters and scaling factors used to compute $B_1$ and J, as well as 10g-averaged specific absorption rate (SAR) of the tuned and matched coils. Post-processing was performed in Matlab (Mathworks, Natick, USA) using a dedicated toolbox (SimOpTx, Research Studio Austria, Medical University of Vienna, Austria) employing the quadratic form power correlation matrix formalism [16,17] for estimation of deposited power in lossy materials by transmit coils.

#### 2.3.3. Experimental evaluation

The MTMG-TLRs for 7 T MRI were fabricated by a third party with standard photolithographic etching techniques (db electronic, Daniel Boeck SAS, Saint-Louis, France). On the bench, the resonance frequencies and Q-factors of the designed structures were measured using the single loop probe method. In experiments, a box shaped phantom (16 × 16 × 9 cm$^3$) filled with polyacrylic acid gel with tissue-like dielectric properties was used as load. The distance between the TLRs and the phantom was 12 mm.

MRI experiments were carried out on a 7 T whole-body MRI system (Magnetom 7 T MRI, Siemens Medical Solutions, Erlangen, Germany). All coils were used in transmit/receive mode. The required transmit-receive switch, and low-noise preamplifier (0.5 dB noise figure, 27.2 ± 0.2 dB gain; Siemens Healthcare, Erlangen, Germany) were placed on a separate interface board. The saturated Turbo FLASH (satTFL) method [18] employing a rectangular slice-selective saturation pulse (2 ms pulse duration, 17.5 V pulse amplitude for the 7 cm loop coil, as well as the 4t10g-3cm and the 5t14g-4cm MTMG-TLR, 25 V pulse amplitude for all other coils) was used to acquire flip angle maps for all coils. The pulse voltage was reduced for those coils which showed very high $B_1^+$ values in simulations in order to limit generated flip angles to the usable range [19]. $B_1^+$ maps normalized to the input power were calculated from measured flip angle distributions taking into account an insertion loss of −1.5 dB of the coil cables and the TR-switch, which was measured on the bench. Finally, MR images of a papaya fruit were acquired using the 5t16g-6cm TLR and a 3D gradient echo sequence ($T_R/T_E$ = 30/2.45 ms, $T_{acq}$ = 15:43 min, 0.33 × 0.33 × 2 mm$^3$ nominal resolution, 128 × 128 × 208 mm$^3$ FOV). Tuning and matching of the TLR on the papaya could be achieved without difficulty by adjusting the respective capacitors in the pick-up loop.

## 3. Results

### 3.1. Prototype study at 4.7 T

The measured resonance frequency of the designed prototype MTMG-TLR is 204.2 MHz when unloaded. The 4t6g TLR could be fine-tuned and matched at the Larmor frequency of 199.8 MHz without difficulty for all loading conditions using the resonant inductive matching setup. Q-factors of 340 for the unloaded flat TLR, 46 for the flat TLR loaded with the planar phantom, 80 for

**Table 1**
MTMG-TLR and loop coil designs for 7 T MRI with corresponding resonance frequencies and quality factors. $d_{ext}$ – external coil diameter, $d_{mean}$ – mean coil diameter, $w$ – conductor width, $p$ – spacing between turns, $n$ – number of turns, $n_g$ – number of gaps, $f_{0u}$ and $f_{0l}$ – resonance frequency of the coil (without pick-up loop) when unloaded and when loaded by the phantom, respectively, $Q_u$ – quality factor of the unloaded coil, $Q_l$ – quality factor of the loaded coil.

| Name | $d_{ext}$ [mm] | $d_{mean}$ [mm] | $w$ [mm] | $p$ [mm] | $n$ | $n_g$ | $f_{0u}$ [MHz] | $f_{0l}$ [MHz] | $Q_u$ | $Q_l$ | $Q_u/Q_l$ |
|---|---|---|---|---|---|---|---|---|---|---|---|
| 4t10g-3cm | 100 | 65.7 | 4.0 | 6.1 | 4 | 10 | 291.8 | 292.5 | 235.3 | 10.8 | 21.9 |
| 5t14g-4cm | 100 | 72.4 | 2.0 | 4.4 | 5 | 14 | 291.2 | 294.0 | 217.7 | 10.0 | 21.8 |
| 2t6g-5cm | 100 | 75.7 | 6.8 | 10.7 | 2 | 6 | 313.1 | 319.0 | 185.3 | 7.1 | 26.6 |
| 5t16g-6cm | 100 | 80.1 | 1.5 | 3.1 | 5 | 16 | 302.1 | 307.0 | 174.3 | 7.1 | 24.6 |
| 2t6g-8cm | 100 | 90.7 | 3.0 | 3.3 | 2 | 6 | 291.3 | 295.0 | 196.0 | 9.5 | 20.6 |
| 7 cm | 71.5 | 70.0 | 1.5 | – | – | – | 301.0 | 303.5 | 299.3 | 17.6 | 17.0 |
| 8 cm | 81.5 | 80.0 | 1.5 | – | – | – | 298.5 | 302.0 | 276.0 | 14.5 | 19.1 |
| 9 cm | 91.5 | 90.0 | 1.5 | – | – | – | 300.5 | 305.0 | 237.0 | 11.8 | 20.1 |

the flat TLR loaded with the cylindrical phantom, and 60 for the TLR form-fitted to the cylindrical phantom were measured.

Gradient echo images acquired with the MTMG-TLR prototype and corresponding SNR maps are depicted in Fig. 2b. It is shown that the novel TLR can be used for MRI and its form-fitting ability is demonstrated. The comparison between flat and bent configuration shows that form-fitting the TLR to the cylindrical phantom leads to an SNR gain not only at the sides of the phantom, but also along the central coil axis (Fig. 2c). For instance, an SNR gain of 20% is observed at a distance of 10 mm inside the phantom.

### 3.2. Comparison study at 7 T

The measured resonance frequencies of the isolated (i.e. without pick-up loop) MTMG-TLRs and conventional loop coils with and without loading are given in Table 1. For the unloaded and loaded loop coils, $f_{0u}$ and $f_{0l}$ are the resonance frequency due to the segmentation capacitors along the loops. The resonance frequency of the loaded 2t6g-5cm TLR (319.0 MHz) is 7% higher than the Larmor frequency (297.2 MHz); for all other MTMG-TLRs the deviation is $\leqslant$3%. Fine-tuning and matching at the Larmor frequency could be achieved for all coils with the resonant inductive matching technique. A drop of the measured quality factor with loading by more than a factor of 17 was observed for all MTMG-TLRs and loop coils (see Table 1). This confirms that coil noise is negligible in comparison to sample noise, as assumed for simulations in this work.

Figs. 3 and 4 summarize the simulation results and experimental data of the study performed at 7 T, including $B_1^+$ maps, a picture of the experimental set-up and an MR image of the papaya fruit. The simulated and measured $B_1^+$ profiles show that the $B_1$ distribution varies strongly among the compared MTMG-TLR designs

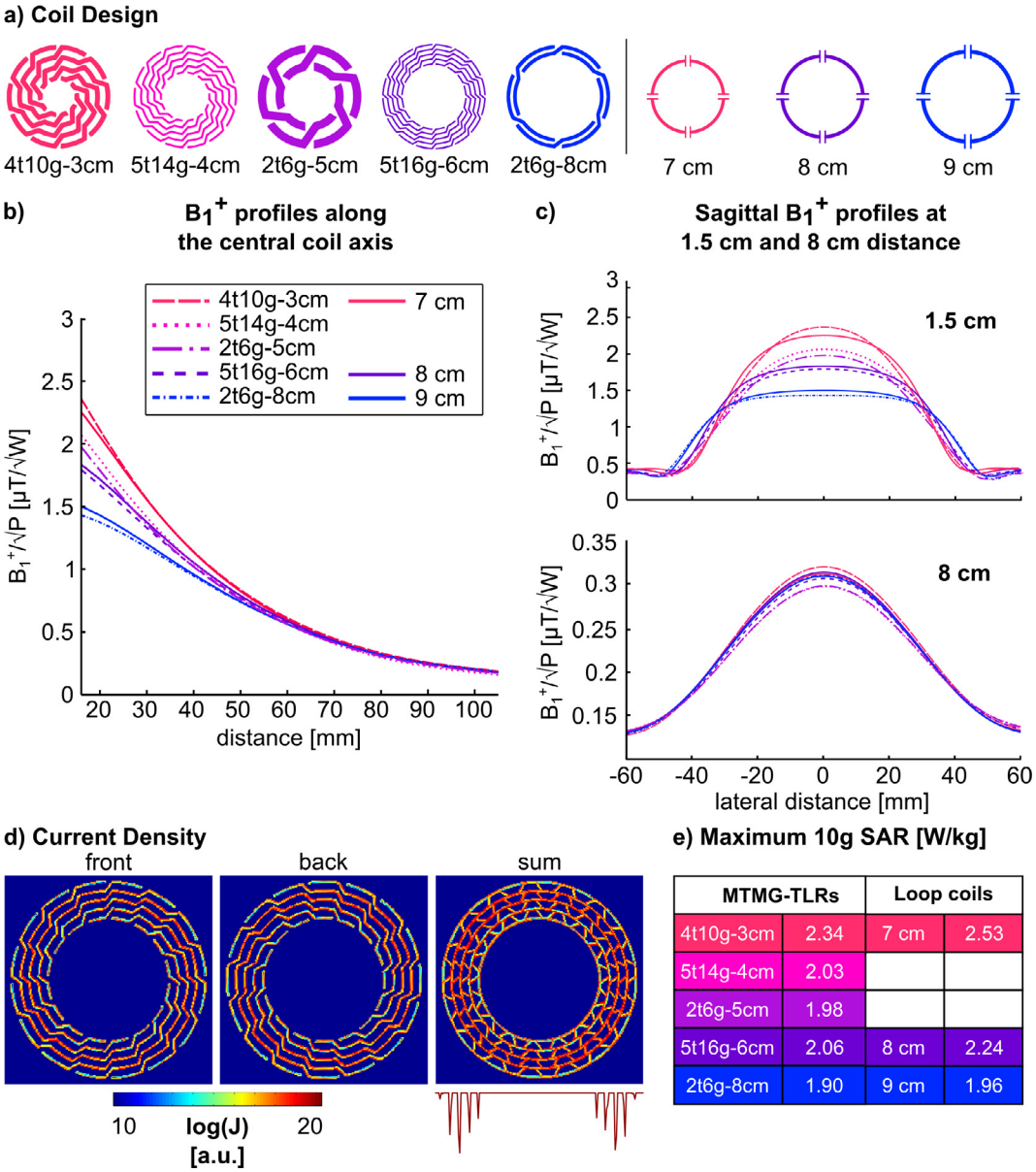


| MTMG-TLRs | | Loop coils | |
|---|---|---|---|
| 4t10g-3cm | 2.34 | 7 cm | 2.53 |
| 5t14g-4cm | 2.03 | | |
| 2t6g-5cm | 1.98 | | |
| 5t16g-6cm | 2.06 | 8 cm | 2.24 |
| 2t6g-8cm | 1.90 | 9 cm | 1.96 |

**Fig. 3.** Simulation results of the comparison study at 7 T. (a) Compared coil designs. Only the front conductor is shown for MTMG-TLRs. Loop coils are labeled according to their diameter. Same colors of MTMG-TLRs and loops indicate similar $B_1^+$ distributions. (b) Central axis profiles of the simulated $B_1^+$ fields for 1 W input power. (c) Sagittal $B_1^+$ profiles for 1 W input power at 1.5 cm and 8 cm distance from the coils. (d) Simulated current density distribution for the 5t16g-6cm TLR in front and back conductors on a logarithmic scale, sum of the current density TLR in front and back conductors, and current profile across the individual turns. (e) Maximum 10g-averaged SAR (the same color code as in a–c is used). (For interpretation of the references to color in this figure legend, the reader is referred to the web version of this article.)

(Figs. 3b, c and 4a, b). The 2t6g-5cm and the 5t14g-4cm TLRs produce a high $B_1^+$ over a narrow lateral FOV in the region close to the coil, which decreases rapidly along the coil axis. The 2t6g-8cm TLR generates a lower $B_1^+$ but over a broader FOV and larger penetration depth; the $B_1^+$ profile of the 5t16g-6cm TLR appears to represent a compromise between the former two configurations. The 4t10g-3cm TLR, on the other hand, combines high superficial $B_1^+$ and large penetration depth; this MTMG-TLR shows the highest $B_1^+/\sqrt{P}$ for all depths (Fig. 3b and c).

When comparing the $B_1^+$ profiles of MTMG-TLRs and loop coils (Fig. 3b and c), it can be observed that the MTMG-TLRs generate a $B_1^+$ field, which is roughly comparable to that of a loop with the mean diameter = (outer diameter + inner diameter)/2 of the MTMG-TLR. This indicates that the overall behavior of an MTMG-TLR is dominated by its central turns, which can be explained by looking at the current density distribution along the TLR (Fig. 3d). Fig. 3d depicts the currents in front and back conductors as well as their respective sum; the $B_1$ field of the TLR is generated by the common mode current, proportional to the sum of the currents flowing in the two conductors. This current is constant along each turn due to the gaps placed alternatingly along the two conductors. However, the central turns of the MTMG-TLR experience a higher current density than the outer and inner turns. This results from the fact that the MTMG-TLR is composed of several conductive strips ranging from the outermost to the innermost turn (Fig. 1d), with maximum current at the center of the individual strips and minimum current at their respective ends (Fig. 3d).

From Fig. 3b and c it can be seen that the $B_1^+$ profiles of the 4t10g-3cm, the 5t16g-6cm, and the 2t6g-8cm TLRs are roughly comparable to those of the 7 cm, the 8 cm and the 9 cm loop coils, respectively. While the $B_1^+$ amplitude of the 5t16g-6cm TLR is 2–3% lower than that of the 8 cm loop, the 2t6g-8cm TLR shows lower $B_1^+$ close to the coil, but higher $B_1^+$ at larger depths (>5 cm). Contrarily, the 4t10g-3cm TLR performs slightly better than the 7 cm loop in terms of $B_1^+/\sqrt{P}$ for all depths; interestingly, this TLR also shows higher $B_1^+$ values at large depth than the larger loop coils. This indicates that the contribution of the outer turns of the MTMG-TLRs to the generated $B_1$ increases in comparison to the inner turns for large distances. Therefore, MTMG-TLRs can behave more similar to larger loop coils for large distances, depending on their design.

Maximum 10g-averaged SAR values are shown in Fig. 3e. In comparison to loop coils, the MTMG-TLRs show lower maximum

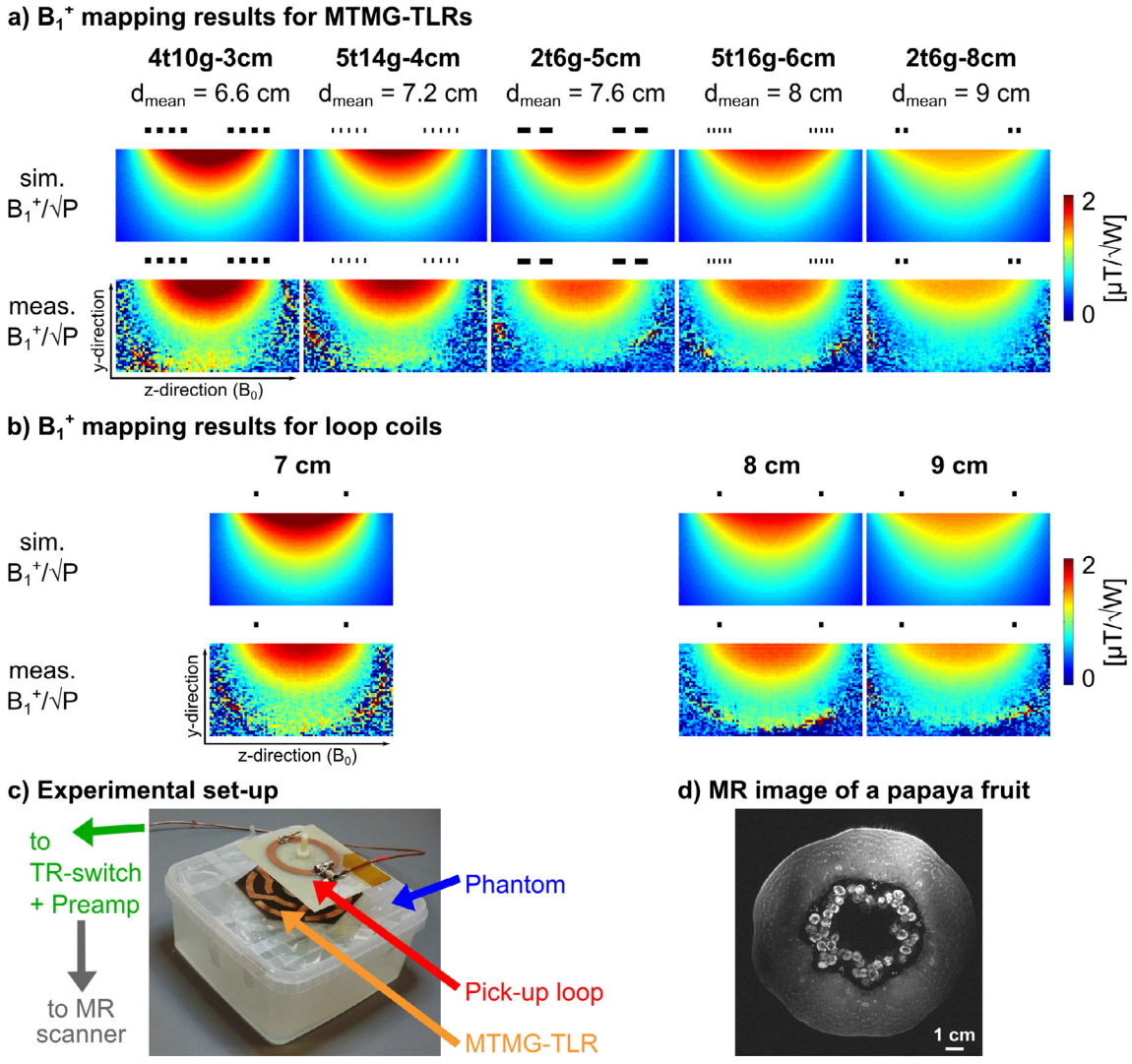


**Fig. 4.** Measurement results of the 7 T study. (a and b) Comparison of simulated and measured $B_1^+$ distributions at 7 T for the MTMG-TLRs and loop coils, respectively. Sagittal $B_1^+$ maps for 1 W input power, as well as normalized $B_1^+$ distributions calculated from measured flip angle maps are shown. The black bars above the $B_1^+$ maps indicate the positions of the conductors. (c) Picture of the experimental set-up showing the positioning of an MTMG-TLR and the pick-up loop on the phantom. (d) Transversal GRE image of a papaya fruit acquired with the 5t16g-6cm TLR ($T_R/T_E$ = 30/2.45 ms, $T_{acq}$ = 15:43 min, 0.33 × 0.33 × 2 mm$^3$ nominal resolution, 128 × 128 × 208 mm$^3$ FOV).

10g-averaged SAR values at comparable $B_1^+$ efficiency, e.g. the 4t10g-3cm and the 5t16g-6cm TLRs have approximately 8% lower maximum 10g-averaged SAR values than the 7 cm and the 8 cm loop coil, respectively. Also the low maximum 10g-averaged SAR values of the 5t14g-4cm and the 2t6g5cm TLRs with regard to their high $B_1^+$ efficiency in the region close to the coil should be noted.

The experimental $B_1^+$ maps (Fig. 4a and b) deduced from acquired flip angle maps are in good qualitative and quantitative agreement with simulations; deviations in the order of ±10–15% are observed for regions with sufficient image SNR. Out of the five investigated MTMG-TLRs, the highest deviations between simulation and experiment are observed for the 2t6g-5cm TLR. This can be explained by the high resonance frequency of the TLR (i.e. 319 MHz), which requires a large frequency shift generated by resonant inductive matching. This increases the pick-up loop noise factor and therefore reduces the $B_1^+$ efficiency of the complete set-up consisting of pick-up loop and TLR [4]. As the coils were modeled as lossless components in simulations, this effect is only observable in the measured $B_1^+$ maps, and not in the simulation results.

## 4. Discussion

In this work, the novel MTMG-TLR design has been introduced and evaluated at two different field strengths, 4.7 T and 7 T. In the prototype study at 4.7 T it has been demonstrated that MRI is feasible with MTMG-TLRs. Further, it has been shown that form-fitting the MTMG-TLR to a phantom with a non-planar surface leads to a significant SNR gain in comparison to the same coil used in flat configuration. The possibility of form-fitting presents one of the advantages of TLRs, since no solder joints, which might break upon bending, are required for coil tuning.

In the 7 T study, five different MTMG-TLRs have been compared regarding their $B_1^+$ and SAR performance in EM simulations and MRI experiments. Strong variations in $B_1^+$ distribution between the five MTMG-TLR designs have been observed. This reveals the high potential of the MTMG-TLR design. The $B_1$ distribution of a TLR strongly depends on the number and the distribution of turns. However, up to now the number of turns could not be chosen freely, but was constricted by the desired TLR diameter and resonance frequency, resulting in very limited options for $B_1$ optimization. With the novel MTMG-TLR design, the effect of the number of turns and the diameter on the resonance frequency can be compensated for by adjusting the number of gaps. Therefore, these parameters can now be chosen freely (within practical limits set by the fabrication process). The additional degree of freedom was directly exploited in this work by designing MTMG-TLRs with an external diameter of 10 cm for 7 T MRI. This TLR diameter and resonance frequency could not have been achieved with the single-gap multi-turn TLR design.

Also, a comparison to standard loop coils with diameters ranging from 7 to 9 cm was performed. It could be concluded that, as a rule of thumb, MTMG-TLRs produce a $B_1^+$ field that is comparable to that of a loop coil with the mean diameter of the MTMG-TLR. Subtle differences occur depending on the MTMG-TLR design and the current distribution resulting therefrom. On the other hand, lower SAR values were observed for MTMG-TLRs in comparison to their corresponding loop coils. Since power and SAR scale with the square of RF pulse amplitudes, even a small reduction may allow for significant improvements to data quality by reducing pulse durations, e.g. lower chemical shift displacement in spectroscopy [20], higher SNR due to shorter echo times. Alternatively, the duty cycle can be increased, e.g. shorter repetition delays [21] or longer echo trains in multi spin echo sequences. This list of potential benefits is exemplary only, definitely not complete.

In principle, single-turn TLRs with the same mean diameter as an MTMG-TLR could be produced to generate a similar $B_1$ field but at the price of severe design limitations. For single-turn TLRs, changing $n_g$ by ±1 causes a large change of the resonance frequency, due to the, as a first approximation, linear relationship between $\omega_0$ and $n_g$. Therefore, choosing $n_g$ as a free design parameter, gives access only to a discrete spectrum of frequency bands for single-turn TLRs. The remaining design parameters, namely the conductor width and the substrate properties, often cannot be chosen in a way to achieve exactly the desired mean TLR diameter. With the MTMG-TLR design these limitations can be overcome, since the number of turns and the spacing between turns become available as additional design parameters.

In this work, MTMG-TLRs with constant inter-turn spacing were investigated. In future studies, also the MTMG-TLR designs with variable spacing between individual turns could be tested. This could be useful to optimize, for example, the $B_1$ homogeneity at a certain depth.

For biomedical applications, a suitable coil housing, that incorporates the MTMG-TLR and the pick-up loop, has to be developed. The housing has to ensure patient safety and the mechanical stability of the set-up, as the distance between TLR and pick-up loop has to be fixed in order to maintain the matching condition. Further considerations about a suitable housing are required when the MTMG-TLR should be used as geometrically adjustable coil; a potential solution is presented by combining rigid and flexible housing materials, e.g. vinyl fabric [22], or PTFE.

In future work, also, the applicability of the novel MTMG-TLR design for RF coil arrays will be investigated. Recently, first studies on decoupling techniques suitable for TLRs including overlapping annexes [23] and shielding rings [24] have been performed. Of these two techniques, the latter is very promising for MTMG-TLRs since it does not depend on the current distribution along the TLR. This way, several MTMG-TLRs, each surrounded by a shielding ring, could be arranged to form an array either along one or two dimensions. As MTMG-TLRs are inductively matched, one pick-up loop would be required for each element of the array. In this case, care must be taken to limit the interaction between the pick-up loops with each other, while maintaining sufficient coupling between MTMG-TLR and pick-up loop for matching [23].

## 5. Conclusions

A novel design scheme for TLRs has been presented - the MTMG-TLR design. This design enables the construction of TLRs with multiple turns and multiple gaps at the same time, adding a degree of freedom in TLR design. This can be used to overcome current limitations regarding geometry and operating frequency. High-field applications requiring a large FOV can now be addressed with multi-turn TLR design. Also, low-frequency applications of small TLRs benefit from the possibility of more accurate and flexible geometry optimization.

The new flexibility in TLR design should enable the construction of improved RF coils for SAR demanding high field applications, like localized MR spectroscopy, thanks to the lower SAR values and the potential SNR gain due to form-fitting.

## Acknowledgments

The authors acknowledge financial support from the Austrian/French FWF/ANR Programme Blanc grant, Nr. I1371-B24, “FLEXAR7”, and the Austrian/French OeAD/MAEE projects WTZ/PHC Amadée FR08/2013 and FR10/2015.

## References


[1] P. Gonord, S. Kan, A. Leroy-Willig, Parallel-plate split-conductor surface coil: analysis and design, Magn. Reson. Med. 6 (1988) 353–358.

[2] P. Gonord, S. Kan, A. Leroy-Willig, C. Wary, Multigap parallel-plate bracelet resonator frequency determination and applications, Rev. Sci. Instrum. 65 (1994) 3363–3366.

[3] S. Serfaty, N. Haziza, L. Darrasse, S. Kan, Multi-turn split-conductor transmission-line resonators, Magn. Reson. Med. 38 (1997) 687–689.

[4] J.-C. Ginefri, A. Rubin, M. Tatoulian, M. Woytasik, F. Boumezbeur, B. Djemaï, et al., Implanted, inductively-coupled, radiofrequency coils fabricated on flexible polymeric material: application to in vivo rat brain MRI at 7 T, J. Magn. Reson. 224 (2012) 61–70.

[5] L. Darrasse, J.-C. Ginefri, Perspectives with cryogenic RF probes in biomedical MRI, Biochimie 85 (2003) 915–937.

[6] E. Laistler, M. Poirier-Quinot, S. Lambert, R.-M. Dubuisson, O.M. Girard, E. Moser, et al., In vivo MR imaging of the human skin at sub-nanoliter resolution using a superconducting surface coil at 1.5 T, J. Magn. Reson. Imaging 41 (2015) 496–504.

[7] S. Eroglu, B. Gimi, B. Roman, G. Friedman, R.L. Magin, NMR spiral surface microcoils: design, fabrication, and imaging, Concepts Magn. Reson. 17B (2003) 1–10.

[8] M. Burian, M. Hájek, Linear microstrip surface coil for MR imaging of the rat spinal cord at 4.7 T, Magn. Reson. Mater. Phys. Biol. Med. 17 (2004) 359–362.

[9] V. Ramaswamy, J.W. Hooker, R.S. Withers, R.E. Nast, W.W. Brey, A.S. Edison, Development of a $^{13}$C-optimized 1.5-mm high temperature superconducting NMR probe, J. Magn. Reson. 235 (2013) 58–65.

[10] P.B. Roemer, W.A. Edelstein, C.E. Hayes, S.P. Souza, O.M. Mueller, The NMR phased array, Magn. Reson. Med. 16 (1990) 192–225.

[11] J. Mispelter, M. Lupu, A. Briguet, NMR Probeheads for Biophysical and Biomedical Experiments: Theoretical Principles and Practical Guidelines, Imperial College Press, London, 2006.

[12] J.-C. Ginefri, E. Durand, L. Darrasse, Quick measurement of nuclear magnetic resonance coil sensitivity with a single-loop probe, Rev. Sci. Instrum. 70 (1999) 4730–4731.

[13] M. Kozlov, R. Turner, Fast MRI coil analysis based on 3-D electromagnetic and RF circuit co-simulation, J. Magn. Reson. 200 (2009) 147–152.

[14] R.A. Lemdiasov, A.A. Obi, R. Ludwig, A numerical postprocessing procedure for analyzing radio frequency MRI coils, Concepts Magn. Reson. Part A 38A (2011) 133–147.

[15] A. Kumar, W.A. Edelstein, P.A. Bottomley, Noise figure limits for circular loop MR coils, Magn. Reson. Med. 61 (2009) 1201–1209.

[16] I. Graesslin, H. Homann, S. Biederer, P. Börnert, K. Nehrke, P. Vernickel, et al., A specific absorption rate prediction concept for parallel transmission MR, Magn. Reson. Med. 68 (2012) 1664–1674.

[17] A. Kuehne, S. Goluch, P. Waxmann, F. Seifert, B. Ittermann, E. Moser, et al., Power balance and loss mechanism analysis in RF transmit coil arrays, Magn. Reson. Med. 74 (2015) 1165–1176.

[18] S. Chung, D. Kim, E. Breton, L. Axel, Rapid $B_1^+$ mapping using a preconditioning RF pulse with TurboFLASH readout, Magn. Reson. Med. 64 (2010) 439–446.

[19] R. Pohmann, K. Scheffler, A theoretical and experimental comparison of different techniques for $B_1$ mapping at very high fields, NMR Biomed. 26 (2013) 265–275.

[20] M. Meyerspeer, T. Scheenen, A.I. Schmid, T. Mandl, E. Unger, E. Moser, Semi-LASER localized dynamic $^{31}$P magnetic resonance spectroscopy in exercising muscle at ultra-high magnetic field, Magn. Reson. Med. 65 (2011) 1207–1215.

[21] F. Niess, G.B. Fiedler, A.I. Schmid, S. Goluch, R. Kriegl, M. Wolzt, et al., Interleaved multivoxel $^{31}$P MR spectroscopy, Magn. Reson. Med. Epub (2016), http://dx.doi.org/10.1002/mrm.26172.

[22] M.A. Erturk, A.J.E. Raaijmakers, G. Adriany, K. Ugurbil, G.J. Metzger, A 16-channel combined loop-dipole transceiver array for 7 T body MRI, Magn. Reson. Med. Epub (2016), http://dx.doi.org/10.1002/mrm.26153.

[23] R. Kriegl, J.-C. Ginefri, M. Poirier-Quinot, L. Darrasse, S. Goluch, A. Kuehne, et al., Novel inductive decoupling technique for flexible transceiver arrays of monolithic transmission line resonators, Magn. Reson. Med. 73 (2015) 1669–1681.

[24] M.H. Deppe, J. Parra-Robles, H. Marshall, T. Lanz, J.M. Wild, A flexible 32-channel receive array combined with a homogeneous transmit coil for human lung imaging with hyperpolarized $^3$He at 1.5 T, Magn. Reson. Med. 66 (2011) 1788–1797.